ADVANCED MATERIALS
www.advmat.de

Enhanced Resonance for Facilitated Modulation of Large-Area Perovskite Films with Stable Photovoltaics

Ligang Xu, Haodong Ji, Wei Qiu, Xin Wang, Yan Liu, Yuanhao Li, Jing Li, Xin Zhang, Daiquan Zhang, Jiexue Wang, Ye Tao, Meicheng Li,* and Runfeng Chen**

Upscaling efficient and stable perovskite films is a challenging task in the industrialization of perovskite solar cells partly due to the lack of high-performance hole transport materials (HTMs), which can simultaneously promote hole transport and regulate the quality of perovskite films especially in inverted solar cells. Here, a novel HTM based on N–C = O resonance structure is designed for facilitating the modulation of the crystallization and bottom-surface defects of perovskite films. Benefiting from the resonance interconversion (N–C = O and N^+ = C–O^-) in donor-resonance-donor (D-r-D) architecture and interactions with uncoordinated Pb^{2+} in perovskite, the resulting D-r-D HTM with two donor units exhibits not only excellent hole extraction and transport capacities, but also efficient crystallization modulation of perovskite for high-quality photovoltaic films in large area. The D-r-D HTM-based large-area (1.02 cm^2) devices exhibit high power conversion efficiencies (PCEs) up to 21.0%. Moreover, the large-area devices have excellent photo-thermal stability, showing only a 2.6% reduction in PCE under continuous AM 1.5G light illumination at elevated temperature (≈65 °C) for over 1320 h without encapsulation.

1. Introduction

Inverted perovskite solar cells (IPSCs) have attracted considerable attention due to their simple operation, negligible hysteresis, good operational stability, and high compatibility with tandem or flexible architectures.[1–3] However, although the highest power conversion efficiency (PCE) of IPSCs has over 25%, the device area is generally less than 0.1 cm^2, which lags far behind the silicon cells (> 100 cm^2). Besides, intrinsic instability remains a big hinder for the large-area IPSCs to realize commercialization. The biggest challenge in depositing large-area perovskite films for highly stable IPSCs is owing to the numerous defects (including ion vacancies, antisites, and interstitial defects) of perovskite generated during device fabrication and operation, leading to light and heat-induced degradation in large-area

L. Xu, W. Qiu, X. Wang, Y. Liu, X. Zhang, D. Zhang, Y. Tao, R. Chen
Key Laboratory for Organic Electronics and Information Displays (KLOEID) & Jiangsu Key Laboratory for Biosensors, Institute of Advanced Materials (IAM)
Nanjing University of Posts & Telecommunications
9 Wenyuan Road, Nanjing 210023, China
E-mail: iamytao@njupt.edu.cn; iamrfchen@njupt.edu.cn

L. Xu
Wuhan National Laboratory for Optoelectronics
Huazhong University of Science and Technology
1037 Geyu Road, Wuhan, Hubei 430074, China

H. Ji, Y. Li
School of Environment and Energy
Peking University Shenzhen Graduate School
1120 Lianhua Road, Shenzhen 518055, China

Y. Li
Department of Civil and Environmental Engineering
Carnegie Mellon University
Pittsburgh, PA 15213, USA

The ORCID identification number(s) for the author(s) of this article can be found under https://doi.org/10.1002/adma.202301752

DOI: 10.1002/adma.202301752

J. Li
Key Laboratory of Photochemical Conversion and Optoelectronic Materials
Technical Institute of Physics and Chemistry
Chinese Academy of Sciences
29 Zhongguancun east road, Beijing 100190, China

J. Wang
College of Chemistry and Life Science
Sichuan Provincial Key Laboratory for Structural Optimization and Application of Functional Molecules
Chengdu Normal University
4 Baishou Road, Chengdu 611130, China

M. Li
State Key Laboratory of Alternate Electrical Power System with Renewable Energy Sources
School of New Energy
North China Electric Power University
2 Beinong Road, Beijing 102206, China
E-mail: mcli@ncepu.edu.cn

R. Chen
School of Materials Science and Engineering
Zhejiang Sci-Tech University
Hangzhou 310018, China

IPSCs.[4,5] And the operating stability under the standard illumination (1-sun) at elevated temperatures is the important test conditions for their future applications. Thus, the suppression defects at interfaces and grain boundaries of the large-area perovskite film is required to improve the efficiency and intrinsic stability of PSCs.[6] To reduce defects of perovskite films, most research has focused on stabilizing the perovskite top surface through post-treatment[7] and surface passivation,[8,9] whereas the bottom-surface of perovskite is less noted,[10] although the bottom surfaces have even more defects (particularly deep charge traps) than the top surfaces.[11] And, light is from perovskite bottom-surface in IPSCs which makes it more vulnerable to degradation. Therefore, it is crucial to reduce the defects of perovskite film at both the top and bottom surfaces for constructing large-area stable IPSCs.

Perovskite films were usually fabricated on the top surface of hole-transporting material (HTM), which generally acts as hole transporting layer in IPSCs and would have significant effects on the quality of perovskite films.[12–16] Excellent HTMs should have the following characteristics: suitable energy levels, high hole mobility, photochemical stability, and orthogonal solubility.[17] Further, HTMs are expected to contribute to reducing the bottom-surface defects by forming favorable molecular interactions with the uncoordinated ions of perovskite. Lewis base functional groups can provide electrons to ion vacancies and repair defects by forming coordination bonds that reduce the activity of the defects;[5,6,18,19] such principles can be used to design HTMs that have an increased capacity for the passivation of bottom-surface defects. Poly(triarylamine) (PTAA) is a widely used HTM for small-area IPSCs (< 0.1 cm^2) owing to its good energy level alignment and film properties.[12] However, PTAA has a poor wettability with very few nucleation sites for perovskite crystallization and poor interface properties of PTAA/perovskites.[14,20] Moreover, owing to the lack of suitable functional groups to interact with perovskite surface, PTAA only has the capacity for hole transportation without noticeable capacity for the repair of bottom-surface defects, resulting in relatively poor efficiencies and stability in large-area IPSCs.[21] Recently, self-assembled monolayer (such as MeO-2PACz) was introduced as HTM for small-area IPSCs with boosting the efficiency of IPSCs over 24%. MeO-2PACz contains an anchoring group bonding to the ITO surface and a functional headgroup for tuning surface properties.[6,22,23] However, there is little exploration in upscaling IPSC technology by using self-assembled monolayer.[21,24] Therefore, it is urgent to develop high-performance and multifunctional HTMs, which can simultaneously support good hole transport, perovskite crystallization modulation, and the interface defects passivation, for the access permission of large-area stable IPSCs.

Smart organic semiconductors with self-adaptive properties have been viewed as promising materials for various high-performance organic optoelectronic devices.[25,26] Resonance structures with different ways of depicting a compound in two or more possible bonding structures could modulate its electronic properties by differing the distributions of electrons upon external stimuli.[25] Organic molecules with resonance structures capable of redistributing electrons on different atoms through resonance interconversion (neutral structure and polarized canonical forms) might enhance the interaction with the uncoordinated Pb^{2+} and halide ionic vacancies defects during perovskite crystallization.[14,27,28] Recently, our group utilized a HTM molecule of CzPFO with N–P = O resonance structures in donor-resonance-acceptor (D-r-A) structure for IPSCs, resulting in a high PCE of 21.9% (<0.1 cm^2) due to its resonance interconversion induced perovskite crystallization modulation.[14] But, the high energy difference (1.69 eV) between neutral N-P = S and polarized N^+-P = S^- of CzPFO might not modulate the bottom-surface defects sufficiently to improve the perovskite crystallization and enlarge the scalability of the resultant IPSCs. In principle, an ideal organic molecule with resonance structure should have an almost barrier-free and fast resonance interconversion[29,30]; such a property would improve resonance interconversion and permit the construction of high-quality films via the modulation of perovskite crystallization and bottom-surface defects. Therefore, HTMs with a smaller energy difference between neutral structure and polarized canonical forms could facilitate much enhanced coordination interactions that can be used for tuning crystallization and bottom-surface defects, which is the key to obtaining high-quality large-area perovskite films.

Here, we develop an efficient molecule of 4-(10*H*-phenoxazin-10-yl)phenyl)(9*H*-carbazol-9-yl)methanone (CzCOPXZ) in donor-resonance-donor (D-r-D) molecular configuration with the highest occupied molecular orbital (HOMO) energy level of -5.21 eV and high mobility of 2.4×10^{-5} cm^2 V^{-1} S^{-1} for the 1.02-cm^2 large-area stable IPSCs. This molecule is prepared via an economic, facile, and scalable synthesis to combine the two donors of carbazole and phenyl-phenoxazine together with N-C = O resonance structures. CzCOPXZ possesses a good wettability for perovskite deposition and a small energy difference (0.59 eV) between neutral N-C = O and polarized N^+-C = O^- for the improvement resonance interconversion through electron redistribution, which will enhance the interaction with uncoordinated Pb^{2+} and halide ionic vacancies in modulating perovskite crystallization. In addition, this HTM induces vertical perovskite growth for the reduced grain boundaries and energy losses. Moreover, the D-r-D molecule with two efficient donor units contributes significantly to enhancing hole extraction and transport capacities. As a result, 1.02 cm^2 IPSCs with D-r-D CzCOPXZ-based HTM show an improved efficiency up to 21.0%. Furthermore, the device displays state-of-the-art long-term photo-thermal stability, retaining 97.4% of its initial PCE after continuous 1-sun illumination at 65 °C over 1300 h. The improved stability should be due to the unique modulation of large-area perovskite films, which permits the construction of high-quality large-area perovskite films and high-performance devices for future industrialization.

2. Results and Discussion

The CzCOPXZ molecule in a D-r-D structure was designed to facilitate modulation of perovskite films and to promote the hole extraction and transport by double linking of two donor units for stable and efficient large-area photovoltaics (**Figure 1**a). The donor of phenoxazine unit was used to improve the HTM film formation and hole-transporting properties. Another donor unit of carbazole has been also considered as an efficient terminal group in HTM designs due to its excellent hole-transporting

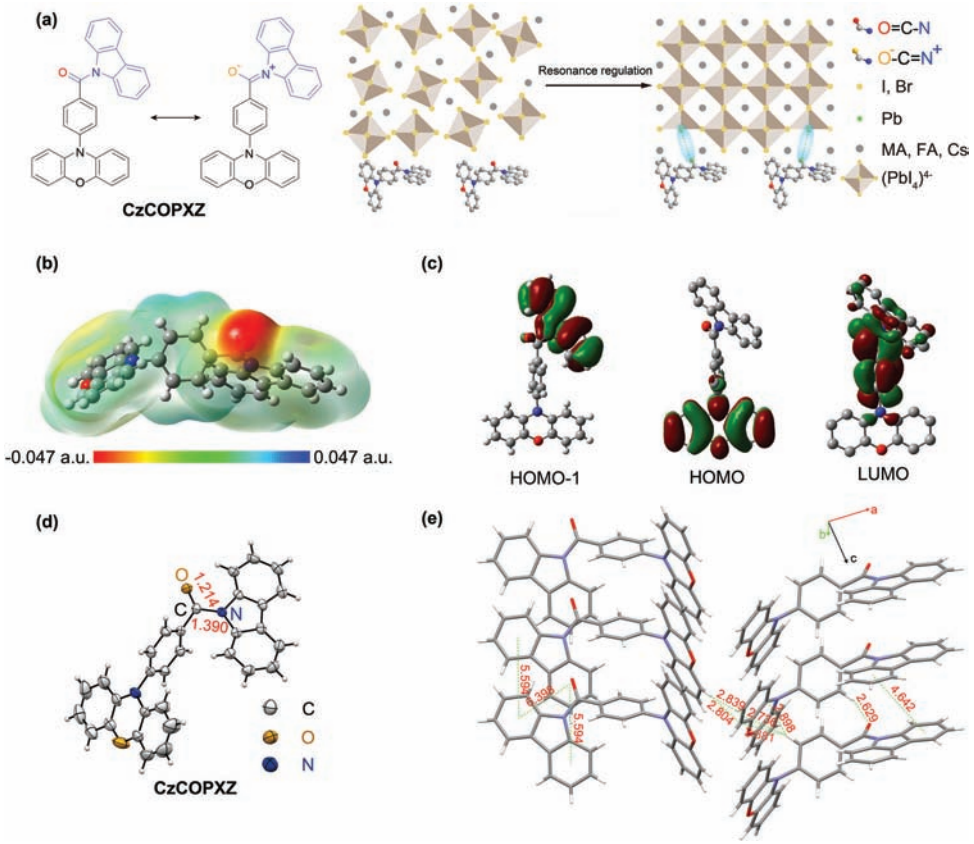

Figure 1. a) CzCOPXZ with resonance structure of for modulation of perovskite crystallization and bottom-surface defects healing. b) Calculated electrostatic potential surface map of CzCOPXZ. c) Frontier molecular orbital distributions of CzCOPXZ by B3LYP/6-31G(d, p). d) Single-crystal structure of CzCOPXZ. e) Molecular packing motifs in CzCOPXZ single crystal.

ability, high degree of electron donation, and low cost.[31,32] The benzophenone unit was selected as the middle π-bridge for an intense intermolecular stacking.[33] More importantly, since the perovskite crystalizes process is not in the exact solid state due to the presence of residual solvent, the N–C = O group with resonance interconversion (N–C = O and N^+ = C–O^-) forms to act as Lewis bases can efficiently repair the uncoordinated Pb^{2+} defects and modulate the perovskite crystallization at the earliest stage (Figure 1a). Therefore, CzCOPXZ with a D-r-D molecular configuration permits the easy tuning of the energy levels for high-performance solar devices. Meanwhile, compared to D-r-A molecule of CzPFO, the D-r-D molecule with two efficient donor units contribute significantly to enhance the hole extraction and transport capacities. CzCOPXZ was easily synthesized via an Ullmann reaction with a good total yield of up to 69% (Scheme S1, Supporting Information). The synthesis details and characterizations are provided in Figures S1–S3 (Supporting Information).

The electronic properties of CzCOPXZ were evaluated via both theoretical and experimental studies. Based on calculated electrostatic potential surface (EPS), abundant negative potential exists around the N-C = O resonance structure (Figure 1b), facilitating the chemical interaction between the uncoordinated Pb^{2+} and O atoms to form favorable chemical bonds at perovskite bottom interfaces[14] (Figure 1a). CzCOPXZ exhibits a HOMO energy level of -5.17 eV close to that of perovskite (≈5.4 eV), which facilitates the hole extraction from perovskite films and reduces energy loss (Figure 1c). The lowest unoccupied molecular orbital (LUMO) was calculated to be -2.87 eV, which could block electron transport for suppressed the charge recombination in the HTM. The calculated HOMO matches well with that obtained from the cycle voltammetry (CV) measurement (-5.21 eV) (Figure S4, Supporting Information). From the absorption and steady-state photoluminescence (PL) spectra shown in Figure S5 (Supporting Information), it can be found that the CzCOPXZ film can efficiently absorb light with a wavelength from 250 to 450 nm, and the emission peak at 600 nm is in the range of the absorption of the perovskite.[34]

To understand the resonance interconversion and molecular packing of the CzCOPXZ, a single-crystal X-ray diffraction (XRD) analysis was undertaken. From the single crystal configuration (Figure 1d,e), CzCOPXZ crystallizes in a monoclinic structure. The distance between two adjacent molecules is quite small (less than 3 Å), suggesting the strong intermolecular interactions and compact molecular packing. This packing structure also favors hole transport. The measured N–C bond length in CzCOPXZ is 1.390 Å (Figure 1d), which is significantly shorter than the normal N–C bond length (1.445 Å).[30] And the C = O bond length (1.214 Å) in CzCOPXZ is longer than its standard length (1.200 Å),[30] indicating the existence resonance interconversion between N–C = O and N^+ = C–O^- forms. From the bond

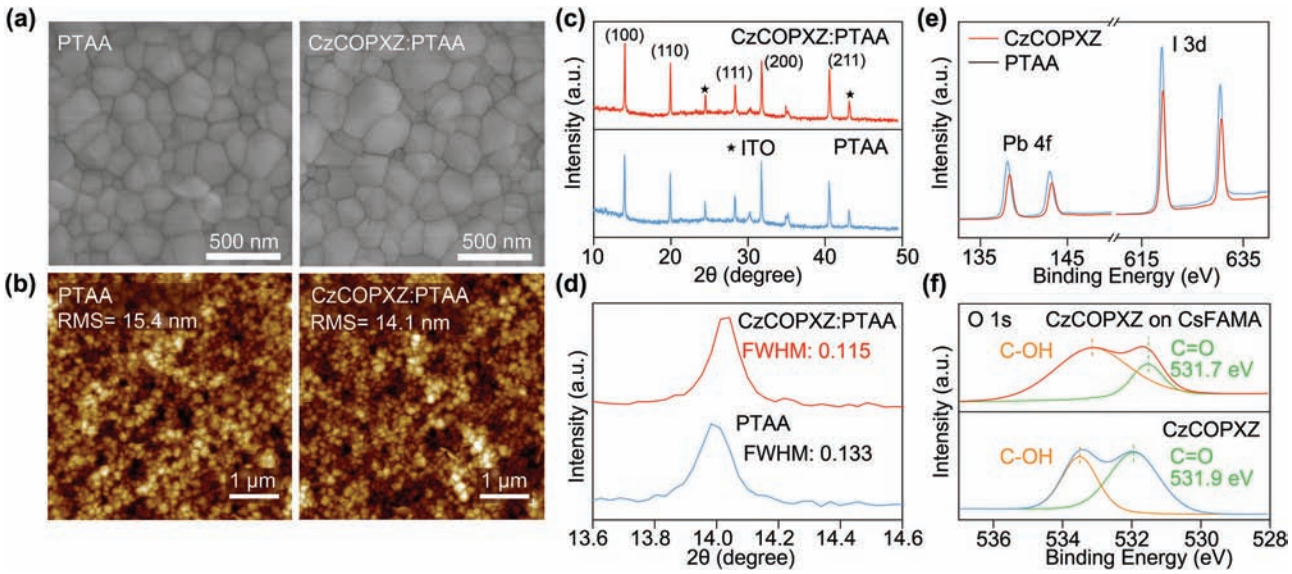

Figure 2. a) SEM and b) AFM images of CsFAMA films deposited on PTAA and CzCOPXZ:PTAA-based HTM layers. c) XRD patterns with d) magnification at 2θ from 13.6° to 14.6°. e,f) XPS spectra of e) Pb 4f and I 3d for normal perovskite and CzCOPXZ-modulated perovskite and f) O 1s of pure CzCOPXZ and CzCOPXZ on perovskite.

order analysis,[29] the increased N–C (1.216) and reduced C = O (1.965) bond orders also verify the resonance structure. The energy difference between the N–C = O and N^+ = C–O^- forms of CzCOPXZ was also obtained by calculating the energy difference between the idealized natural Lewis structures of N^+ = C–O^- and N–C = O.[29,35] A much lower energy (0.59 eV) than that of N–P = O (1.69 eV) was observed, which could facilitate defects reparation of uncoordinated Pb^{2+} for large-area high-quality perovskite films.[29]

In light of the suitable energy level and excellent resonance interconversion properties of CzCOPXZ, the molecule was employed as the HTM in IPSCs. Compared with a PTAA layer (Figure S6, Supporting Information), the pure CzCOPXZ layer shows a worse film-forming property with a larger root mean square (RMS) roughness (4.47 nm). However, after doping with a small amount of PTAA (20 wt.%), the CzCOPXZ:PTAA composite film shows a significantly reduced RMS roughness of 1.06 nm (Figure S6, Supporting Information), suggesting that PTAA doping effectively promotes molecule stacking to form compact HTM layer for avoiding the immediate contact between perovskite and electrode for reducing recombination. We then used PTAA-doped CzCOPXZ composite films as the HTM in IPSCs. First, we determined the conductivities of the PTAA and CzCOPXZ:PTAA films by considering the current–voltage (I–V) characteristics of the devices with the indium tin oxide (ITO)/HTM/Al structure (Figure S7, Supporting Information). The conductivity values of the PTAA and CzCOPXZ:PTAA HTMs were 6.70×10^{-4} and 1.23×10^{-3} mS cm^{-1}, respectively. Then we further investigated the hole mobilities (μ_h) using the space charge-limited current (SCLC) method based on hole-only devices with the ITO/HTM/MoO_3/Al structure (Figure S8, Supporting Information). The value of μ_h for the CzCOPXZ:PTAA film was estimated to be 2.41×10^{-5} cm^2 V^{-1} s^{-1}, which represents a twofold increase compared with that of the pure PTAA (1.20×10^{-5} cm^2 V^{-1} s^{-1}). Therefore, compared with PTAA films, the CzCOPXZ:PTAA has significantly improved conductivity and hole mobility, which should contribute to enhancing the hole transport in the devices. The water contact angles of PTAA and the CzCOPXZ:PTAA films suggest that the CzCOPXZ-derived HTM is more hydrophilic (contact angle of 69°) than PTAA (90°). Thus, CzCOPXZ:PTAA could be more suitable for use in polar perovskite solutions, as it facilitates perovskite nucleation and growth (Figure S9, Supporting Information).

We further study the effects of the CzCOPXZ:PTAA on the crystallization of the $(Cs_{0.05}FA_{0.81}MA_{0.14})Pb(I_{0.86}Br_{0.14})_3$ (CsFAMA) film. Based on the acquired scanning electron microscopy (SEM) images, the CsFAMA film on the CzCOPXZ:PTAA film has a larger average grain size of 240 nm compared with that of 180 nm measured for the control CsFAMA film (**Figure 2**a; Figure S10, Supporting Information). Moreover, the atomic force microscopy (AFM) images of a 5.0 × 5.0 μm^2 area on the surface of the CsFAMA film indicate that the RMS roughness of the films grown on PTAA and the CzCOPXZ:PTAA film were 15.4 and 14.1 nm, respectively (Figure 2b). The XRD patterns show that the perovskite crystal on the CzCOPXZ:PTAA film exhibits a notably increased ratio of the peak associated with the (100) planes to the peaks associated with the other crystal planes (Figure 2c); this finding indicates that a preferred crystal orientation of perovskite crystal with the aid of CzCOPXZ. In addition, the CzCOPXZ-derived perovskite film has a lower full width at half maximum (FWHM) of the (100) diffraction peak (0.113) than the control films (0.133), supporting the observation that CzCOPXZ:PTAA induces a better crystallization with a larger crystallite size than PTAA (Figure 2d). Moreover, the ultraviolet (UV) absorption spectrum of the CzCOPXZ-derived perovskite was obtained to confirm the crystal quality of the sample (Figure S11, Supporting Information). The mechanism for improving the perovskite quality could be proposed. The introduction of hydrophilic CzCOPXZ molecule in the HTMs has better affinity to the polar perovskite precursor, which can

facilitate the nucleation and growth of perovskite crystals. Importantly, the Lewis base group (N–C = O) could efficiently interact with the perovskite, leading to a dense, smooth, pinhole-free perovskite film with reduced interfacial defects. Therefore, CzCOPXZ with the N–C = O resonance structure might improve defect reparation of the uncoordinated Pb^{2+} ions in bottom interface during crystallization for high-quality perovskite film.

Then, X-ray photoelectron spectroscopy (XPS) was used to investigate whether chemical interactions between CzCOPXZ and the perovskite exist. It was found that the energy of the Pb 4f level shifted up by 0.3 eV compared with that observed in the control perovskite sample; this finding indicates the formation of a favorable chemical interaction between CzCOPXZ and the Pb atoms of the perovskite (Figure 2e). The Pb:I ratios were also calculated for the CsFAMA and CsFAMA/CzCOPXZ layers. It was found that the Pb:I ratio of the CsFAMA/CzCOPXZ layer was reduced from 1:3.61 to 1:3.45, indicating that there were less uncoordinated Pb^{2+} ions due to the chemical interaction between CzCOPXZ and the perovskite.[36] The characteristic peak of O 1s (corresponding to the carboxyl group) was found to shift from 531.9 eV in the CzCOPXZ film to 531.7 eV in CzCOPXZ film on the perovskite (Figure 2f), which further confirms the chemical interaction between the CzCOPXZ and the perovskite and the formation of Pb–O chemical bonds.[37,38]

Based on the molecular dynamics (MD) simulations, the radial distribution function (RDF) (or pair distribution function) was used to elucidate the structural properties of the sample at equilibrium, which can distinguish the phase behavior and determine the structural factor/thermodynamic properties of materials.[39] The RDF is obtained from the following expression:

$$g(r) = \frac{N(r + dr) - N(r)}{4\pi r^2 \rho dr} \quad (1)$$

where g represents the RDF, r is the interparticle separation distance. The Buckingham–Coulomb potential was used to accurately model the charged ions (Figure S12, Supporting Information); this model considers both the long-range Coulomb interaction and the short-range Buckingham potential.

The RDF indicates the probability of finding a particle at a distance r from a given reference atom. The RDF value is 0 for values of r close to 0, indicating that there is no atom within a small distance due to the excluded volume. The first peak of the RDF curve corresponds to the distance of the nearest neighbor; the value of this peak is roughly equal to the value of the parameter σ in the Lennard–Jones potential[40,41] (the lattice constant in the solid phase). The second and subsequent peaks indicate that there are more neighboring atoms considered in this counting process (**Figure 3**a). The peak locations of the initial peaks of the RDF curves are the same for the perovskite with either more or less Pb. The RDF eventually converges to 1 for large values of r, which describes the infinite atoms in the counting range. The difference in the RDF between the systems with varying Pb content is that the perovskite structure with a high Pb content converges to 1 faster than the perovskite with a low Pb content. Given the same RDF curve of the Pb–Pb interaction between the two atomic structures, this difference in the convergence rates is caused by the interactions between Pb and O (Figure 3a). The Pb-rich structure has a significantly closer distance of Pb-O with 2.39 Å than

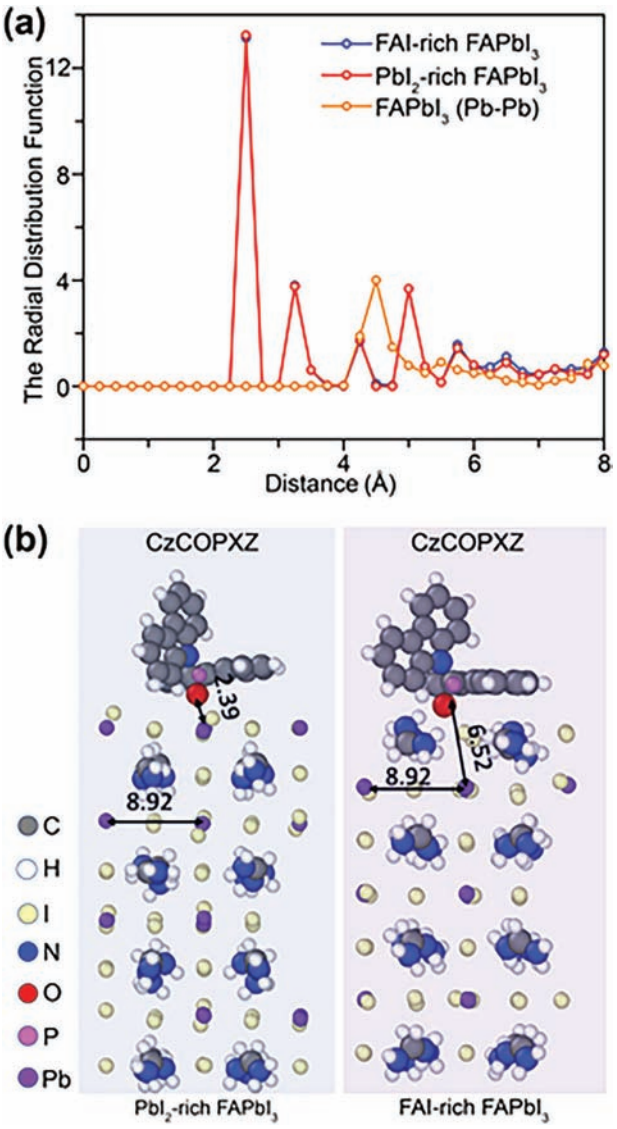

Figure 3. a) Radial distribution function at 300 K using the Buckingham–Coulomb potential of the equilibrated structures with 50 bins. b) Optimized equilibrium structures and interactions between CzCOPXZ and PbI_2-rich (left) and FAI-rich (right) $FAPbI_3$.

FAI-rich structure compared with 6.52 Å for the structure with a less Pb) (Figure 3b). The C–O distances in CzCOPXZ for the FAI-rich and Pb-rich surfaces of the perovskite are 2.83 and 2.91 Å, respectively, which shows that the CzCOPXZ could vary the C–O distance to repair the Pb^{2+} defects based on resonance interconversion between N–C = O and N^+ = C–O^-. Furthermore, compared with the FAI-rich perovskite surface, the Pb–O distance for Pb-rich perovskites is closer for stronger long-range interactions (Figure 3b; Figure S13, Supporting Information), which makes the overall structure more stable at the simulation temperature than the pristine perovskite. These findings suggest that CzCOPXZ molecules could also improve the intrinsic device stability.

Encouraged by the above findings related to CsFAMA films on CzCOPXZ:PTAA surfaces, we fabricated a

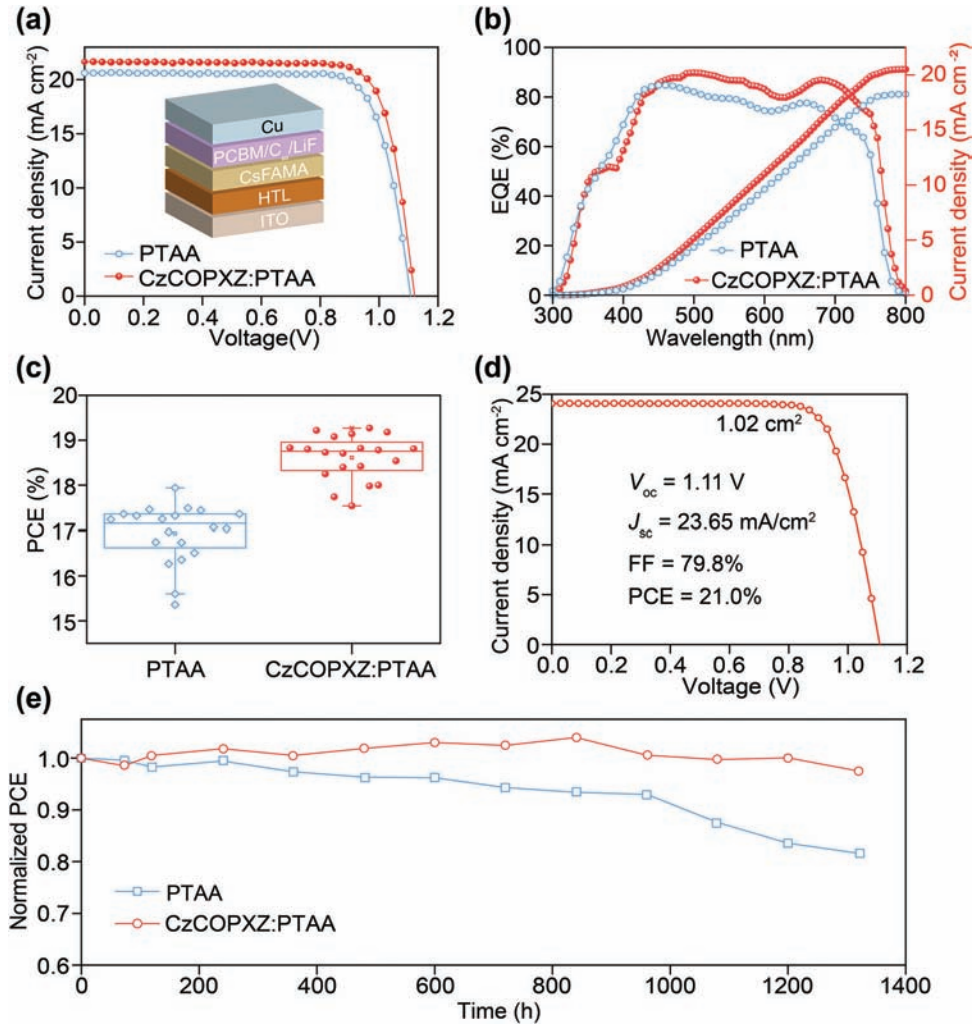

Figure 4. a) *J–V* curves of the IPSCs under AM1.5 G illumination; the inset image shows the device structure. b) EQEs and integrated J_{sc} values of the devices. c) Statistical results of the device parameters and d) performance of the best performing large-area (1.02 cm^2) device subjected to PEAI post-treatment. e) Photo-thermal stability under 1-sun illumination at a temperature of 65 °C

large-area IPSC using the following device structure: ITO/HTM/CsFAMA/PCBM/C_{60}/LiF/Cu (**Figure 4**a; Figure S14, Supporting Information). From the current density–voltage (*J–V*) curves (Figure 4a; Table S1, Supporting Information), it can be seen that the best performing IPSC based on CzCOPXZ:PTAA reaches a PCE of up to 19.3% compared with that of 17.9% of the PTAA-based devices. The stabilized PCE at the maximum power point was measured to have a steady-state short-circuit current (J_{sc}) of 21.65 mA cm^{-2} and a stabilized PCE of up to 18.8% (Figure S15, Supporting Information). We measured 20 devices to investigate the reproducibility of the IPSCs based on CzCOPXZ:PTAA (Figure 4b) and found that the CzCOPXZ:PTAA-derived devices exhibit a good reproducibility and a higher average PCE (18.8%) than the control devices (17.1%). We also investigated the external quantum efficiency (EQE) of the CzCOPXZ:PTAA-based IPSCs (Figure 4c) and found that the integrated J_{sc} value is consistent with the J_{sc} obtained from the *J–V* curves. The CzCOPXZ:PTAA-based IPSC shows a negligible hysteresis in the *J–V* curves in both the reverse and forward scans (a hysteresis index of 0.008 was measured, see Figure S16, Supporting Information). To further improve the device performance, we treated the top surface of the perovskite with PEAI for post-treatment. The best performing device with an aperture area of 1.02 cm^2 was found to exhibit a PCE of up to 21.0% with an open-circuit voltage (V_{oc}) of 1.11 V, a J_{sc} of 23.65 mA cm^{-2}, and a fill factor (FF) of 79.8% (Figure 4d), which is among the highest PCE obtained for $IPSC_S$ with active area ≥1.0 cm^2 (Table S3, Supporting Information). The IPSC based on PEAI treatment also exhibits a negligible hysteresis (hysteresis index of 0.014) (Figure S17, Supporting Information).

The long-term intrinsic photo-thermal stability of the unencapsulated devices was also investigated under a 1-sun illumination in an open-circuit configuration (at 65 °C) in a nitrogen atmosphere (following the ISOS-L-2I protocol). The evolution of the PCE as a function of time is shown in Figure 4e. The CzCOPXZ:PTAA-based device shows excellent photo-thermal stability, and it is seen to outperform the PTAA-based device, maintaining 97.4% of its initial PCE over a 1320-h continuous

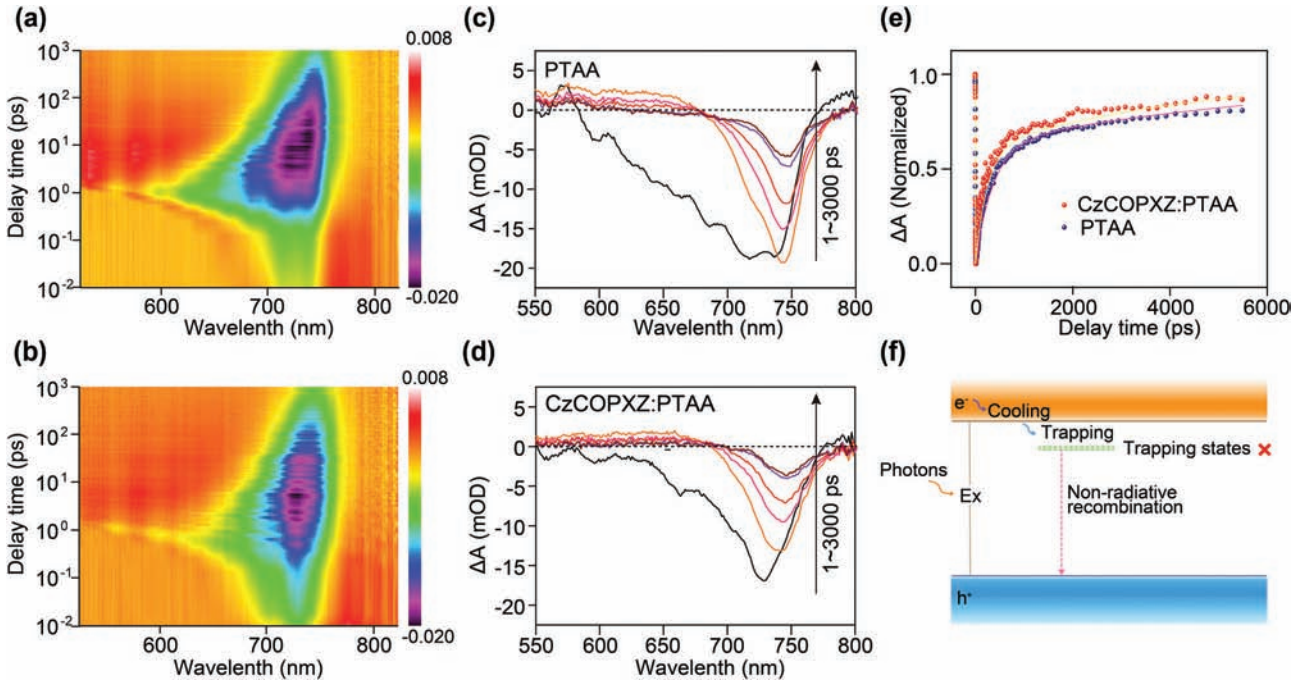

Figure 5. Pseudocolor TAS spectra of a) the PTAA/perovskite film and b) the CzCOPXZ:PTAA-derived perovskite film. c,d) The corrected femtosecond TAS of the perovskite film with different HTMs at selected probe delay time. e) TAS of the perovskite film as a function of the delay time. f) Diagram of the hypothesized processes for the reduced exciton trapping and non-radiative recombination.

illumination period. The good hole transport properties and suitable energy levels of the CzCOPXZ:PTAA ensure an efficient hole extraction, which can effectively limit the thermodynamic driving force for phase separation in perovskite layer due to light-generated charge.[42] In addition, the high-quality perovskite film and favorable chemical interaction between the N–C = O of CzCOPXZ and the Pb ions could also inhibit ion migration, resulting in long-term photo-thermal stability.[43] The high stability is comparable to the performance of other state-of-the-art devices (Table S4, Supporting Information).

Femtosecond transient absorption spectroscopy (fs-TAS) was also conducted to further explore the interfacial charge dynamics in the excited state using different HTMs. **Figure 5**a,b shows the pseudocolor fs-TAS plot for perovskite films based on PTAA and CzCOPXZ:PTAA, respectively. When excited by the pump pulse, ground-state bleaching (GSB) occurs due to the fact that the holes in the ground state and electrons in the excited state reduce the absorption of the probe photons.[44] The values of ΔA (mOD) for samples based on quartz/PTAA/perovskite and glass/CzCOPXZ:PTAA /perovskite with a series of decay times ranging from 1 to 3,000 ps are shown in Figure 5c,d. Both perovskite films show redshifts in the GSBs as the delay time is increased, which can be attributed to the transition from high to low excitation energies.[45] Compared with the control perovskite sample, the CzCOPXZ:PTAA-derived perovskite film was found to have a much faster decay ratio (69.0% and 78.2% for the control sample and CzCOPXZ:PTAA-derived perovskites, respectively), indicating the superior injection of excited-state carriers of CzCOPXZ:PTAA-derived device compared with PTAA-based device.[46] The quenching of the excited-state charges fitted with a double-exponential function for the perovskite films based on different HTMs is shown in Figure 5e. The ultrafast decay (less than 1 ns) indicates the effective quenching due to interfacial charge extraction and transport, whereas the decays on timescales of >1 ns and <1,000 ns indicate the occurrence of a recombination process in the perovskite films.[45] The CzCOPXZ:PTAA HTM showed a faster decay of the GSB peak at ≈750 nm and decreased from 363 to 245 ps, which can be attributed to the efficient modulation of the high-quality perovskite films, which promote the interfacial extraction and transport and enhance the built-in field. In addition, the long decay time (4.48 vs 6.66 ns) can be assigned to the interfacial charge recombination. The decreased long charge carrier lifetime indicates that CzCOPXZ:PTAA reduces the interfacial charge recombination due to the lower density of surface defects (Figure 4e). The hypothesized charge dynamics are also presented in Figure 5f to further clarify the ultrafast charge trapping and recombination processes. Upon excitement due to the absorption of high-energy photons, an electron will transfer to the conduction band and will then decay to the conduction band edge forming a free exciton. The free exciton may then be trapped by the defects inducing non-radiative recombination, or recombine directly via radiative recombination followed by photon emission. Thus, the CzCOPXZ:PTAA could suppress the free exciton trapped by the defects and promote the radiative recombination.

To further elucidate the hole transfer and extraction between the CzCOPXZ:PTAA and the CsFAMA films, the steady-state PL spectra were obtained, and the PL dynamics were investigated (Figure S18a,b, Supporting Information). The PL intensity for the CzCOPXZ:PTAA-derived CsFAMA film was found to be significantly reduced compared with that of the control film based on PTAA. In addition, the time-resolved PL

spectra fitted with a double-exponential function indicate that the charge lifetime of the perovskite on the CzCOPXZ:PTAA films (60.06 ns) is shorter than that of the perovskite on the PTAA films (75.46 ns), indicating that CzCOPXZ:PTAA significantly improves the hole extraction and transport properties of the resultant structure.[34] Capacitance–voltage (*C*–*V*) and electrical impedance spectroscopy (EIS) measurements were undertaken to evaluate the electrical properties of the CzCOPXZ:PTAA-based IPSCs (Figure S18c, Supporting Information). Using a Mott–Schottky analysis of the *C*–*V* measurements, the built-in potential (V_{bi}) was obtained according to the following equation[47]:

$$\frac{1}{C^2} = \frac{2}{\varepsilon_r \varepsilon_0 e N_a}\left(V - V_{bi} - \frac{K_b T}{e}\right) \quad (2)$$

where C is the capacitance; V_{bi} and V are the built-in potential and the applied voltage, respectively; ϵ_0 and ϵ_r are the vacuum permittivity and the relative dielectric constant, respectively; e is the electron charge; N_a is the carrier concentration; K_b is the Boltzmann constant; T is the temperature. The value of V_{bi} in the CzCOPXZ:PTAA-based devices was estimated to be 0.90 V, which is higher than that of the control devices (0.88 V). The increased value of V_{bi} indicates an enhanced driving force causing charge separation, which suppresses charge recombination.[47] EIS was used to further study the charge transport and recombination resistances at the interface between the perovskite and the CzCOPXZ:PTAA (Figure S18d, Supporting Information). The recombination resistance and junction capacitance determine the middle frequency zone of the semicircle. The recombination resistance of the CzCOPXZ:PTAA-based devices further indicates a more efficient charge extraction and a suppressed charge recombination.[48,49]

Light-dependent J_{sc} and V_{oc} measurements were also conducted to further understand the charge mechanism (Figure S18e,f, Supporting Information). Light-dependent J_{sc} measurements can be used to determine the scaling in the relationship $J_{sc} \propto I^{\alpha}$. In general, values of α close to 1 indicate limited space charge effects.[50] The α values for PTAA and the CzCOPXZ:PTAA-based IPSCs were found to be 0.88 and 0.91, respectively. Moreover, the slope deviation of the light-dependent V_{oc} from the value of $k_b T/q$ to the value of $2k_b T/q$ indicates that the trap-assisted Shockley–Read–Hall recombination dominates in IPSCs. In our case, the corresponding slope values for the control and CzCOPXZ:PTAA-based devices were calculated as $1.21k_b T/q$ and $1.36k_b T/q$, respectively (Figures S18f, Supporting Information). These values indicate that trap-assisted charge recombination is efficiently suppressed at the perovskite/CzCOPXZ:PTAA interface.[51,52] Therefore, the CzCOPXZ:PTAA-based IPSCs have a smaller space charge effect and lower charge recombination losses, which is consistent with the results discussed above.

3. Conclusion

In summary, we have designed and utilized a HTM with N-C = O resonance structure that can modulate the perovskite crystallization and reduce the density of bottom-surface defects and simultaneously for constructing large-area perovskite films. This design is based on a D-r-D type molecule, whose charge redistribution through resonance interconversion between neutral structure and polarized canonical forms can simultaneously induce oriented crystallization of the perovskite and repair the bottom-surface defects via chemical interactions between the resonance structures and the uncoordinated Pb^{2+} ions. Owing to the presence of two efficient donor units, the D-r-D molecular configuration of CzCOPXZ also promotes hole extraction and transport capacity of the HTM. Moreover, CzCOPXZ exhibits a suitable HOMO energy level, good wettability, high hole mobility, and favorable chemical interactions with the CsFAMA films. As a result, the CzCOPXZ:PTAA-based 1.02-cm^2 IPSCs show PCEs up to 21.0%, good long-term photo-thermal stability with a PCE reduction of only 2.6% under 1-sun illumination at 65 °C over a duration of 1320 h. This work demonstrates that the molecules based on N-C = O resonance structure and hole extraction/transport abilities are promising for the construction of active HTMs that can massively control perovskite crystallization and bottom-surface defect regulation, thus providing important guidelines for developing high-performance large-area IPSCs.

Supporting Information

Supporting Information is available from the Wiley Online Library or from the author.

Acknowledgements

L.X. and H.J. contributed equally to this work. This study was supported in part by the National Natural Science Foundation of China (62274094, 22075149, 51972110, 61875090, 91833306, and 22322106), Natural Science Foundation of the Jiangsu Higher Education Institutions (22KJB510011), the State Key Laboratory of Alternate Electrical Power System with Renewable Energy Sources (LAPS22006), the Open Project Program of Wuhan National Laboratory for Optoelectronics (2020WNLOKF012), Beijing Municipal Natural Science Foundation (2222076), the Jiangsu Specially-Appointed Professor Plan, the Six Talent Plan of Jiangsu Province (XCL-049), Huali Talents Program of Nanjing University of Posts and Telecommunications and Nanjing University of Posts and Telecommunications Start-up Fund (NUPTSF) (NY219007), Jiangsu Provincial Government Scholarship for Overseas Studies.

Conflict of Interest

The authors declare no conflict of interest.

Data Availability Statement

The data that support the findings of this study are available from the corresponding author upon reasonable request.

Keywords

inverted perovskite solar cells, large-area perovskite films, photo-thermal stability, resonance interconversion, resonance structures

Received: February 23, 2023
Revised: September 24, 2023
Published online: October 19, 2023

[1] X. Sun, Z. Li, X. Yu, X. Wu, C. Zhong, D. Liu, D. Lei, A. K.-Y. Jen, Z. A. Li, Z. Zhu, *Angew. Chem., Int. Ed.* **2021**, *60*, 7227.
[2] X. Li, W. Zhang, X. Guo, C. Lu, J. Wei, J. Fang, *Science* **2022**, *375*, 434.
[3] X. Zhu, G. Huang, C. Zeng, X. Zhan, Ke Liang, Q. Xu, Y. Zhao, P. Wang, Q. Wang, Q. Zhou, Q. Tao, M. Liu, J. Lei, C. Yan, Y. Shi, *Science* **2022**, *376*, eabl8280.
[4] H. Zhang, Y. Wu, C. Shen, E. Li, C. Yan, W. Zhang, He Tian, L. Han, W.-H. Zhu, *Adv. Energy Mater.* **2019**, *9*, 1803573.
[5] S. Ma, X. Zhang, X. Liu, R. Ghadari, M. Cai, Y. Ding, M. Mateen, S. Dai, *J. Energy Chem.* **2021**, *54*, 395.
[6] C. Li, X. Wang, E. Bi, F. Jiang, S. M. Park, Y. Li, L. Chen, Z. Wang, L. Zeng, H. Chen, Y. Liu, C. R. Grice, A. Abudulimu, J. Chung, Y. Xian, T. Zhu, H. Lai, B. Chen, R. J. Ellingson, F. Fu, D. S. Ginger, Z. Song, E. H. Sargent, Y. Yan, *Science* **2023**, *379*, 690.
[7] J. Xue, R. Wang, Y. Yang, *Nat. Rev. Mater.* **2020**, *5*, 809.
[8] B. Chen, P. N. Rudd, S. Yang, Y. Yuan, J. Huang, *Chem. Soc. Rev.* **2019**, *48*, 3842.
[9] L. Xu, X. Feng, W. Jia, W. Lv, A. Mei, Y. Zhou, Qi Zhang, R. Chen, W. Huang, W. Huang, *Energy Environ. Sci.* **2021**, *14*, 4292.
[10] S. Chen, X. Dai, S. Xu, H. Jiao, L. Zhao, J. Huang, *Science* **2021**, *373*, 902.
[11] Z. Ni, C. Bao, Ye Liu, Qi Jiang, Wu-Q Wu, S. Chen, X. Dai, Bo Chen, B. Hartweg, Z. Yu, Z. Holman, J. Huang, *Science* **2020**, *367*, 1352.
[12] L. Xu, Y. Liu, W. Qiu, Y. Li, H. Wang, M. Li, L. Xian, C. Zheng, Y. Chen, R. Chen, *J. Power Sources* **2021**, *506*, 230120.
[13] L. Xu, H. Wang, X. Feng, Y. Zhou, Y. Chen, R. Chen, W. Huang, *Adv. Photonics Res.* **2021**, *2*, 2000132.
[14] L. Xu, D. Wu, W. Lv, Y. Xiang, Y. Liu, Y. Tao, J. Yin, M. Qian, P. Li, L. Zhang, S. Chen, O. F. Mohammed, O. M. Bakr, Z. Duan, R. Chen, W. Huang, *Adv. Mater.* **2022**, *34*, 2107111.
[15] L. Xu, Y. Li, C. Zhang, Y. Liu, C. Zheng, W. Lv, M. Li, Y. Chen, W. Huang, R. Chen, *Sol. Energy Mater. Sol. Cells* **2020**, *206*, 110316.
[16] W. Lv, Z. Hu, W. Qiu, D. Yan, M. Li, A. Mei, L. Xu, R. Chen, *Adv. Sci.* **2022**, *9*, 2202028.
[17] T. Niu, W. Zhu, Y. Zhang, Q. Xue, X. Jiao, Z. Wang, Y.-M. Xie, P. Li, R. Chen, F. Huang, Y. Li, H.-L. Yip, Y. Cao, *Joule* **2021**, *5*, 249.
[18] S. Tan, T. Huang, I. Yavuz, R. Wang, M. H. Weber, Y. Zhao, M. Abdelsamie, M. E. Liao, H.-C. Wang, K. Huynh, K.-H. Wei, J. Xue, F. Babbe, M. S. Goorsky, J.-W. Lee, C. M. Sutter-Fella, Y. Yang, *J. Am. Chem. Soc.* **2021**, *143*, 6781.
[19] D. W. De Quilettes, S. M. Vorpahl, S. D. Stranks, H. Nagaoka, G. E. Eperon, M. E. Ziffer, H. J. Snaith, D. S. Ginger, *Science* **2015**, *348*, 683.
[20] X. X. Liu, Y. H. Cheng, C. Liu, T. X. Zhang, N. D. Zhang, S. W. Zhang, J. S. Chen, Q. H. Xu, J. Y. Ouyang, H. Gong, *Energy Environ. Sci.* **2019**, *12*, 1622.
[21] M. Li, J. Wu, G. Wang, B. Wu, Z. Sun, S. Xue, Q. Qiao, M. Liang, *J. Energy Chem.* **2020**, *47*, 10.
[22] Q. Jiang, J. Tong, Y. Xian, R. A. Kerner, S. P. Dunfield, C. Xiao, R. A. Scheidt, D. Kuciauskas, X. Wang, M. P. Hautzinger, R. Tirawat, M. C. Beard, D. P. Fenning, J. J. Berry, B. W. Larson, Y. Yan, K. Zhu, *Nature* **2022**, *611*, 278.
[23] W. Peng, K. Mao, F. Cai, H. Meng, Z. Zhu, T. Li, S. Yuan, Z. Xu, X. Feng, J. Xu, M. D. McGehee, J. Xu, *Science* **2023**, *379*, 683.
[24] J. Zeng, L. Bi, Y. Cheng, B. Xu, A. K.-Y. Jen, *Nano Res. Energy* **2022**, *1*, 9120004.
[25] Y. Tao, R. F. Chen, H. H. Li, J. Yuan, Y. F. Wan, H. Jiang, C. L. Chen, Y. B. Si, C. Zheng, B. C. Yang, G. C. Xing, W. Huang, *Adv. Mater.* **2018**, *30*, 1803856.
[26] Ye Tao, C. Liu, Y. Xiang, Z. Wang, X. Xue, P. Li, H. Li, G. Xie, W. Huang, R. Chen, *J. Am. Chem. Soc.* **2022**, *144*, 6946.
[27] L. Xu, W. Qiu, M. Feng, Z. Liang, W. Qian, C. Zhou, D. Zhang, M. Li, W. Lv, Ye Tao, R. Chen, *Small* **2023**, *19*, 2207226.
[28] D. Han, J. Wang, L. Agosta, Z. Zang, B. Zhao, L. Kong, H. Lu, I. Mosquera-Lois, V. Carnevali, J. Dong, J. Zhou, H. Ji, L. Pfeifer, S. M. Zakeeruddin, Y. Yang, Bo Wu, U. Rothlisberger, X. Yang, M. Grätzel, N. Wang, *Nature* **2023**. https://doi.org/10.1038/s41586-023-06514-6
[29] Y. Tao, L. J. Xu, Z. Zhang, R. F. Chen, H. H. Li, H. Xu, C. Zheng, W. Huang, *J. Am. Chem. Soc.* **2016**, *138*, 9655.
[30] He Jiang, Ye Tao, J. Jin, Y. Dai, L. Xian, J. Wang, S. Wang, R. Chen, C. Zheng, W. Huang, *Mater. Horiz.* **2020**, *7*, 3298.
[31] K. Albrecht, K. Yamamoto, *J. Am. Chem. Soc.* **2009**, *131*, 2244.
[32] X. Liu, X. Shi, C. Liu, Y. Ren, Y. Wu, W. Yang, A. Alsaedi, T. Hayat, F. Kong, X. Liu, Y. Ding, J. Yao, S. Dai, *J. Phys. Chem. C* **2018**, *122*, 26337.
[33] S. K. Rajagopal, K. Nagaraj, S. Deb, V. Bhat, D. Sasikumar, E. Sebastian, M. Hariharan, *Phys. Chem. Chem. Phys.* **2018**, *20*, 19120.
[34] L. G. Xu, M. Y. Qian, C. Zhang, W. Z. Lv, J. B. Jin, J. S. Zhang, C. Zheng, M. G. Li, R. F. Chen, W. Huang, *Nano Energy* **2020**, *67*, 104244.
[35] E. D. Glendening, C. R. Landis, F. Weinhold, *J. Comput. Chem.* **2013**, *34*, 1429.
[36] T. Wu, Y. Wang, X. Li, Y. Wu, X. Meng, D. Cui, X. Yang, L. Han, *Adv. Energy Mater.* **2019**, *9*, 1803766.
[37] Y. Wang, T. Wu, J. Barbaud, W. Kong, D. Cui, H. Chen, X. Yang, L. Han, *Science* **2019**, *365*, 687.
[38] S. Yang, S. Chen, E. Mosconi, Y. Fang, X. Xiao, C. Wang, Yu Zhou, Z. Yu, J. Zhao, Y. Gao, F. De Angelis, J. Huang, *Science* **2019**, *365*, 473.
[39] S. Plimpton, *J. Comput. Phys.* **1995**, *117*, 1.
[40] A. Mattoni, A. Filippetti, M. I. Saba, P. Delugas, *J. Phys. Chem. C* **2015**, *119*, 17421.
[41] M. P. Allen, D. J. Tildesley, *Computer simulation of liquids*, Oxford university press, Oxford **2017**.
[42] N. Li, Y. Luo, Z. Chen, X. Niu, X. Zhang, J. Lu, R. Kumar, J. Jiang, H. Liu, X. Guo, B. Lai, G. Brocks, Q. Chen, S. Tao, D. P. Fenning, H. Zhou, *Joule* **2020**, *4*, 1743.
[43] R. Azmi, E. Ugur, A. Seitkhan, F. Aljamaan, A. S. Subbiah, J. Liu, G. T. Harrison, M. I. Nugraha, M. K. Eswaran, M. Babics, Y. Chen, F. Xu, T. G. Allen, A. U. Rehman, C.-L. Wang, T. D. Anthopoulos, U. Schwingenschlögl, M. De Bastiani, E. Aydin, S. De Wolf, *Science* **2022**, *376*, 73.
[44] F. Li, S. Zhou, J. Yuan, C. Qin, Y. Yang, J. Shi, X. Ling, Y. Li, W. Ma, *ACS Energy Lett.* **2019**, *4*, 2571.
[45] W. Z. Xu, Y. Gao, W. J. Ming, F. He, J. Z. Li, X. H. Zhu, F. Y. Kang, J. Y. Li, G. D. Wei, *Adv. Mater.* **2020**, *32*, 2003695.
[46] J. Xia, Y. Zhang, C. Xiao, K. G. Brooks, M. Chen, J. Luo, H. Yang, N. I. D. Klipfel, J. Zou, Y. Shi, X. Yao, J. Chen, J. M. Luther, H. Lin, A. M. Asiri, C. Jia, M. K. Nazeeruddin, *Joule* **2022**, *6*, 1689.
[47] X. Meng, Y. Li, Y. Qu, H. Chen, N. Jiang, M. Li, D.-J. Xue, J.-S. Hu, H. Huang, S. Yang, *Angew. Chem., Int. Ed.* **2021**, *60*, 3693.
[48] L. Xu, C. Zhang, X. Feng, W. Lv, Z. Huang, W. Lv, C. Zheng, G. Xing, W. Huang, R. Chen, *J. Mater. Chem. A* **2021**, *9*, 16943.
[49] Y. Huang, T. Liu, B. Wang, J. Li, D. Li, G. Wang, Q. Lian, A. Amini, S. Chen, C. Cheng, G. Xing, *Adv. Mater.* **2021**, *33*, 2102816.
[50] T. Liu, H. Lai, X. Wan, X. Zhang, Y. Liu, Y. Chen, *Chem. Mater.* **2018**, *30*, 5264.
[51] X. Wang, K. Rakstys, K. Jack, H. Jin, J. Lai, H. Li, C. S. K. Ranasinghe, J. Saghaei, G. Zhang, P. L. Burn, I. R. Gentle, P. E. Shaw, *Nat. Commun.* **2021**, *12*, 52.
[52] T. Ye, X. Wang, K. Wang, S. Ma, D. Yang, Y. Hou, J. Yoon, K. Wang, S. Priya, *ACS Energy Lett.* **2021**, *6*, 1480.

